Graphical abstract

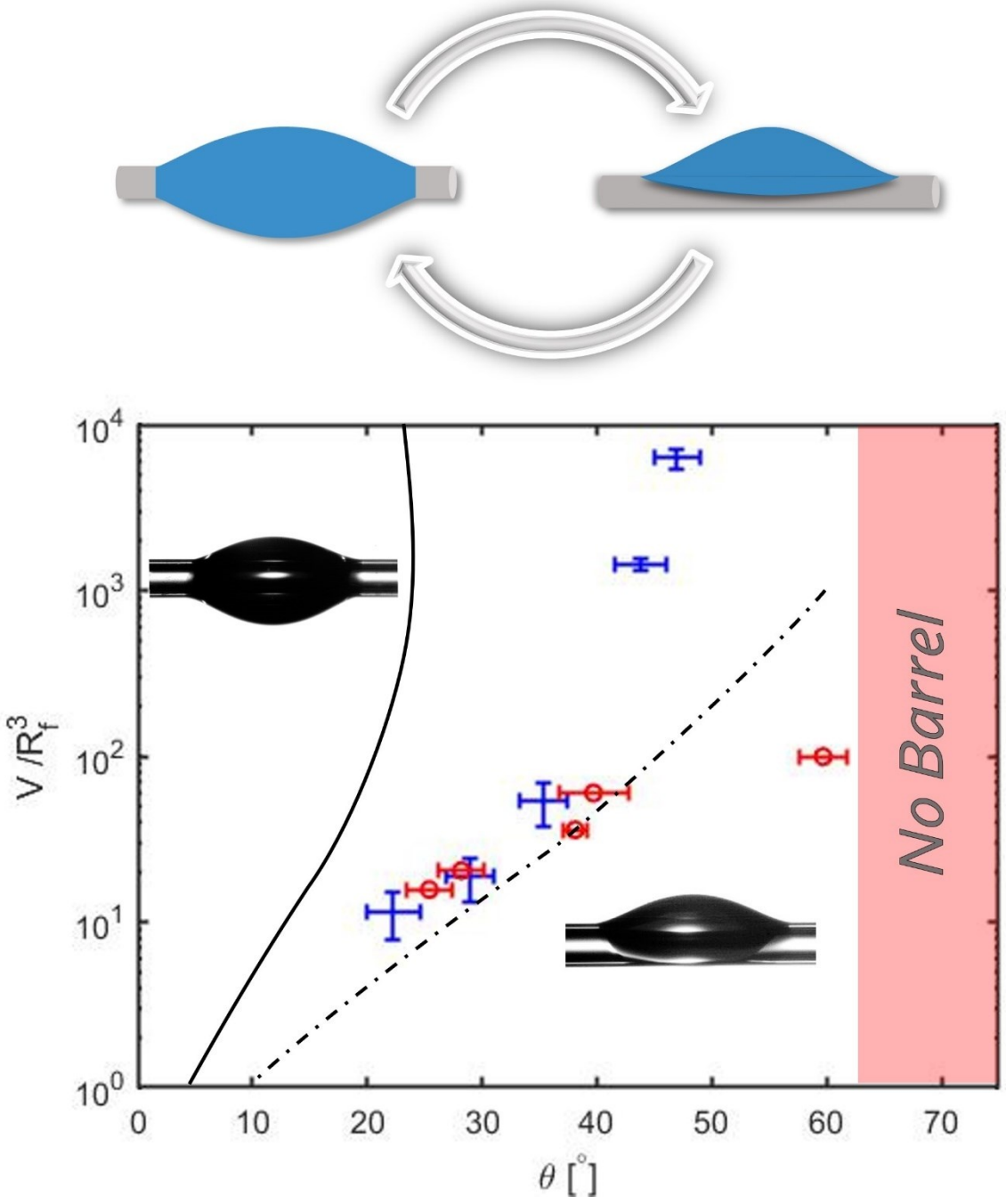

DOES THE CONTACT ANGLE HYSTERESIS CONTROL THE DROPLET SHAPES ON CYLINDRICAL FIBERS?

Yueming Sun and Konstantin G. Kornev

515 Calhoun Drive, 161 Sirrine Hall, Department of Materials Science and Engineering, Clemson University, SC 29634, USA

Corresponding author: Konstantin G. Kornev

Address: *515 Calhoun Drive, 161 Sirrine Hall, Department of Materials Science and Engineering, Clemson University, SC 29634, USA*

Telephone: 864-656-6541
E-mail address: *kkornev@clemson.edu*

Abstract

Hypothesis: Equilibrium droplets on cylindrical fibers are divided in two classes: the barreled and clamshell droplets. In the barreled droplet, the liquid body fully envelops the fiber and the drop forms two boundary contact lines. In the clamshell droplets, some fiber surface under the liquid body remains dry and only one boundary contact line exists. So far, the transition from one shape to the other was predicted by ignoring the contact angle hysteresis. A new series of experiments using the drop-on-demand technology were conducted to analyze the shape of droplets. The existing theory cannot explain the obtained data. We hypothesized that the morphological clamshell-barrel transition of droplets significantly depends on the method of drop formation and is largely controlled by the contact angle hysteresis.

Experiment: To test this hypothesis, we investigated two scenarios of drop formation. In the first scenario, the hexadecane drop was growing on the fiber by printing smaller drops on it. In the second scenario, the drop was formed spontaneously from a coating glycerol film due to the Plateau-Rayleigh instability. To obtain a range of contact angles, a set of different silanes were adsorbed on the fiber surfaces.

Findings: The results showed that for small contact angles ($< 40°$) and small contact angle hysteresis, both methods of drop formation led to the same theoretically explainable conditions for clamshell-barrel transition. As the contact angle increases and hysteresis becomes appreciable, the conditions for clamshell-barrel transition become significantly dependent on the method of drop formation. We discovered that no barreled droplets exist for contact angles greater than 60°. The

experimental results were documented in a set of diagrams describing the clamshell-barrel transitions. These diagrams can be used in different engineering applications.

Keywords

Fiber wetting; capillarity, morphological transition of droplet shapes

1 Introduction

The efficiency of drop collection by the fiber-base absorbers significantly depends on drop shape[1]. On fibers, drops form liquid clamshells or barrels [2] shown in the inserts in Fig.1. The clamshell droplets are easy to shed off a fiber while the barreled droplets firmly adhere to the fiber. It was already known for about 100 years[2-9], that the transformation from clamshell to barrel and back significantly depends on the droplet size relative to the fiber radius and on the wetting properties of fibers. In the existing models [2-12], the wetting properties of fibers are characterized by a single contact angle that the drop makes with the fiber surface. However, when a fiber is immersed in the liquid in question or is withdrawn from it, one observes menisci with distinguishably different contact angles. Thus, the contact angle is not a constant, but it depends on the prehistory of liquid flow. Material engineers wonder which contact angle to choose for design of the fibrous materials such as protection masks, filters or microfluidic devices[1, 3-5, 9, 13-18]?

The contact angle hysteresis is introduced as a difference between the *advancing contact angle* formed when the liquid body moves to wet the fiber surface, and the *receding contact angle* formed when the liquid body recedes back from the wet area. The contact angle hysteresis has never been discussed in the literature on barrel-to-clamshell transformations.

To date, there is only a poor understanding of transformation of clamshell drops to barrel drops or vice versa. This research was pioneered by Carroll [19, 20], who introduced a diagram plotting the

transition boundary between barreled and clamshell droplets in terms of the ratio $n = R_d/R_f$ of the radius R_d of the smallest barrel drop that is going to turn into a clamshell to the fiber radius R_f versus contact angle (θ) that the drop makes with the fiber[20]. Since then, his ideas on this transition have been accepted in the literature[9-12] and this diagram was extensively studied mostly computationally with a few experimental works [6, 7, 9-12, 19-25].

The most popular approach to evaluate the stability condition was proposed by McHale and Newton[22, 25] who directly evaluated the surface free energy of the clamshell drops and the barreled drops by the finite element method using Brakke's Surface Evolver[26]. For the given drop volume and contact angle, the drop conformation should be determined by the lowest possible surface free energy. The results of the numerical experiments were presented in Fig. 1 as the solid lines: the black solid line indicate the boundary of clamshell-to-barrel transition and the red solid line indicates the boundary of barrel-to-clamshell transition. The broken line indicates the condition of equal absolute energy of both states. Plotting this diagram in terms of reduced droplet volume, $V/R^3{}_f$ appears more practically attractive as it allows to predict the drop behavior with little knowledge of the experimental data and hence has an engineering value.

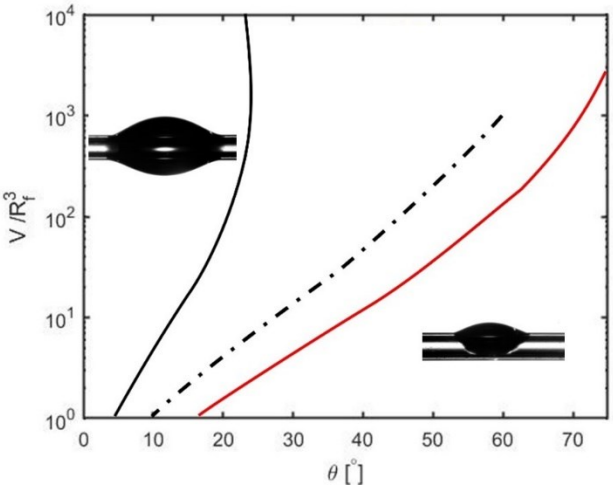

Fig.1. The diagram of the clamshell-barrel transformations numerically obtained in Ref.[9]. The inserts illustrate the shapes of barreled drop and clamshell drops. The black solid line is the boundary when no clamshell droplets could be formed, and the red solid line is the boundary when no barreled droplets could be formed. The broken line indicates the condition of equal absolute energy of the barreled and clamshell droplets.

Mugele's group conducted, probably, the most rigorous experimental analysis of the clamshell-barrel transitions [9]. To change the contact angle *in situ,* the group employed electrowetting phenomenon. The experimental data were compared with numerical modeling to show that the barrel to clamshell transition and the clamshell to barrel transition are governed by different mechanisms. On the diagram in Fig.1, the area between two solid lines was identified as a new bistability region. The group was the first to predict the location of domains of the barreled and clamshell droplets.

The summary of all available results can be drawn as follows: the droplets of nonwetting fluids forming the contact angle $\theta > 90°$, cannot form barrels. For small contact angles and large droplet volumes, the barreled droplets are energetically favorable as their fiber-droplet contact areas are larger than those of the clamshells. In contrast, the clamshells are energetically favorable for large contact angles and small droplet volumes. The drop shape between barreled and clamshell droplets can be changed by temperature[17] or electric potential [9].

In this paper, we experimentally investigate the critical conditions for the transformations of liquid barrels to clamshells and clamshells to barrels. These transformations are studied in the air by changing the method of drop formation. The droplets were formed by two methods. In the first method, the drop was formed by adding one drop on top of the other using the drop-on-demand technology. In the second method, the drop was formed from a coating layer taking advantage of the Plateau-Rayleigh instability[27, 28]. The diagram was studied and compared it with Fig.1. We

confirmed observations of Mugele's group regarding the difference in drop behavior during the transition from clamshell to barrel and from barrel to clamshell[9]. However, the boundaries on the diagram in Fig. 1 appeared different and we never observed axisymmetric barreled drops.

We hypothesize that the contact angle hysteresis is responsible for the shape asymmetry. To check this hypothesis, a detailed high-speed videography was employed. In the drop printing case, the effects of contact angle hysteresis are of primary importance. In the coating method of drop formation, only receding contact angle is important. The scenario of barrel-to-clamshell transition is therefore different.

2. Materials and Methods

2.1. The drops printed on a fiber. Experimental setup and materials

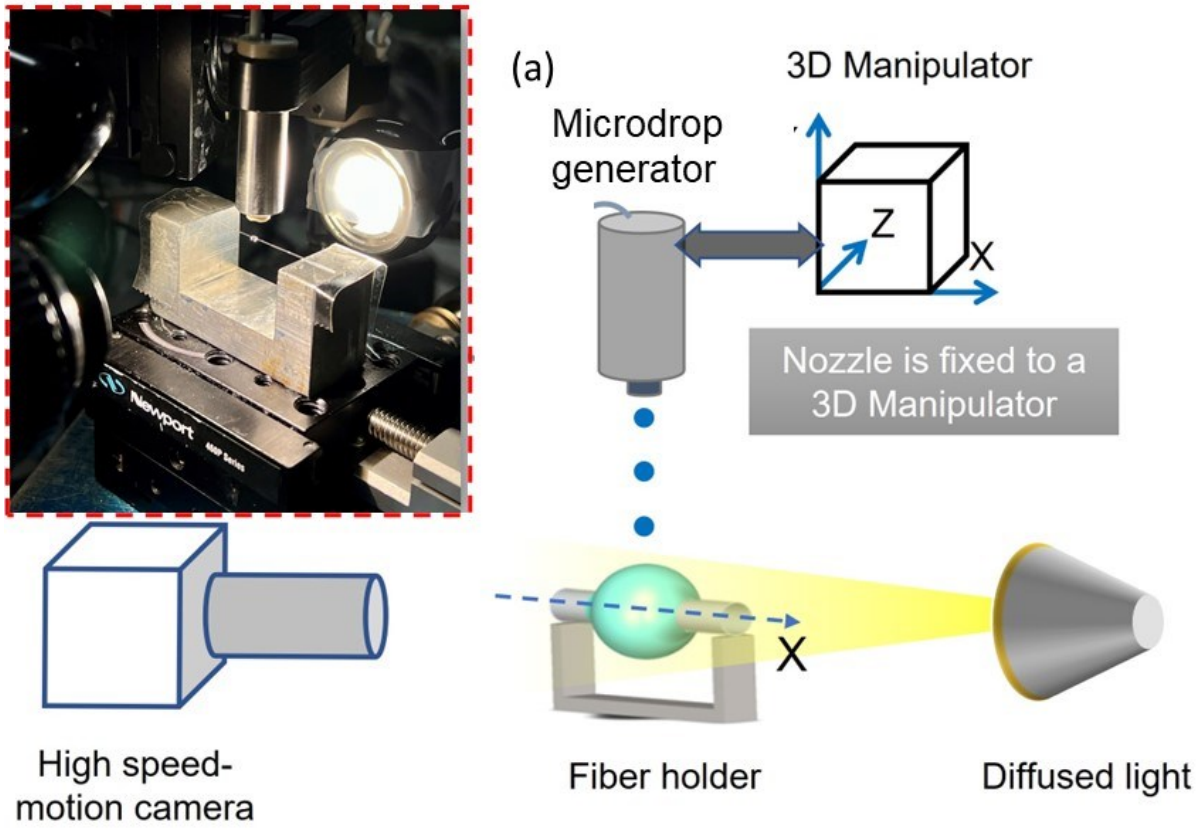

Fig. 2 Schematic of the drop printing setup that consists of three main parts. (i) A microdrop generator controlling the drop size. The drop placement is controlled by a 3D manipulator holding the microdrop generator. (ii) A U-shaped holder with the fiber. The fiber axis is taken as the x-axis of the system of coordinates of manipulator as shown in the picture. (iii) A high speed-motion camera and a diffused light source. The insert shows the actual experimental setup.

The schematic of the experimental system for the drop deposition is shown in Fig. 2(a). The picture of the actual experimental setup is shown in the insert of Fig. 2(a). First, the fiber was mounted on a U-shaped fiber holder, and the holder was attached to a two-dimensional (2D) linear stage. The printing nozzle of the microdrop dispenser (MD-E-201H, Microdrop Technologies)

attached to the three-dimensional (3D) micromanipulator (MP-285 Shutter Instrument Company) was placed about 600 – 800 μm directly above the fiber. The microdrop dispenser was set to generate hexadecane drops of the radius as small as r =13.9 μm every $t_0 = 4950\ \mu s$. Each drop has a volume of about $V_{drop} = 1.13 \times 10^{-5}\ \mu L$. A high speed-motion camera (MotionProY4, Integrated Design Tools, Inc.) with a macro lens (Navitar 1-60135) and a light source (InterTek 4002352) with a diffuser (a piece of a tape) were used to record the process of drop growth on the fiber. The microdrop dispenser has to be calibrated before the experiments to ensure correct settings. The calibration procedure is detailed in Supporting material.

2.2. Drop formation from a coating layer. Experimental setup

The experimental setup for studying drop formation from a coating layer is sketched in Fig. 3 (b). One end of the fiber was attached to a stationary stage. The other end was inserted in a liquid-filled tube attached to a single-axis linear stage (SMC Pollux Microstep Controller). The inner diameter of the tube was 6.1 mm, which is at least one order of magnitude larger than the fiber diameter. When the linear stage was set in motion at the given speed, a coating liquid layer was deposited on the fiber. To deposit a liquid film that is thick enough to form of a big liquid barrel, we used pure glycerol (Glycerin 99.7%, Laboratory Reagent, VWR Chemicals BDH®), the receding contact angles are given in Table 1 and Supporting material.

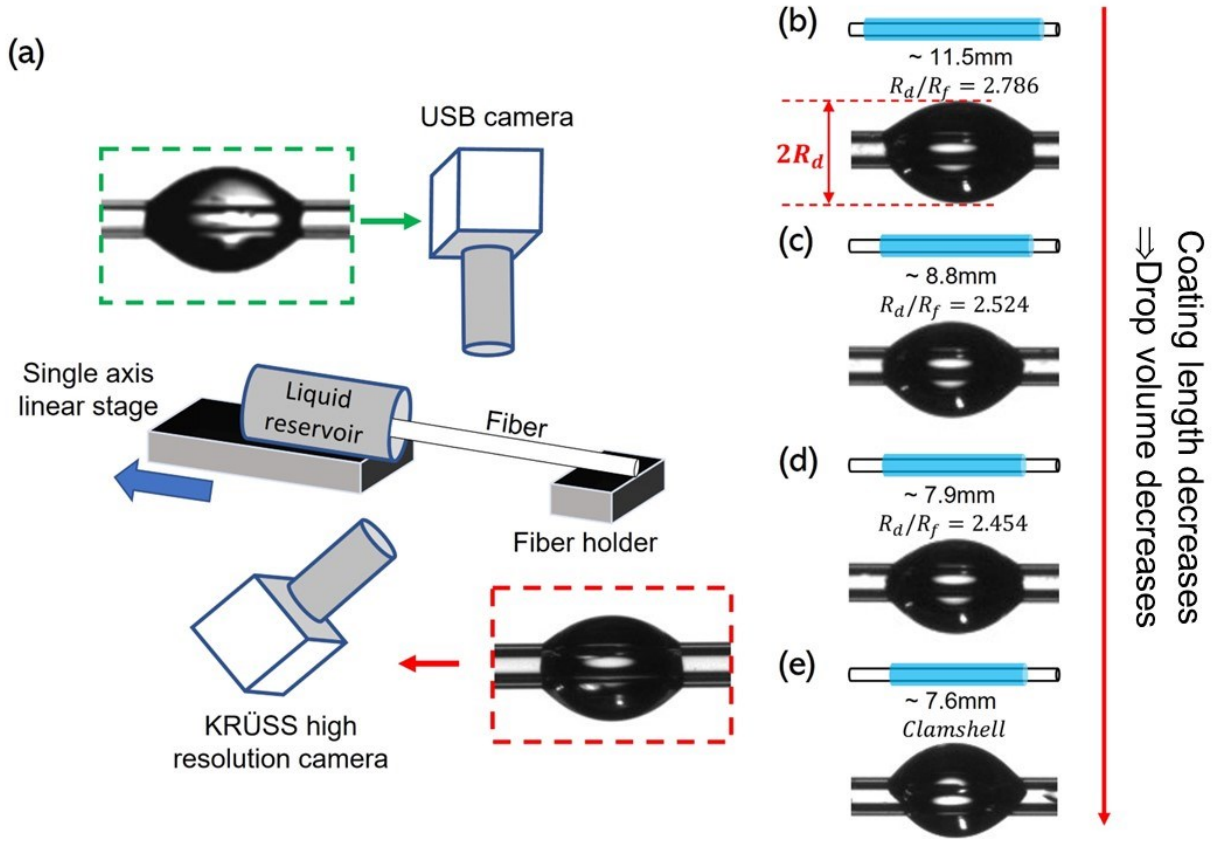

Fig. 3 (a) Schematic of the experimental setup for fiber coating experiments. The fiber is fixed at one end on a holder and its other end is immersed in a liquid-filled tube placed on a linear stage. The fiber gets coated when the stage is set to move at a given velocity. Two cameras film the drop formation process from different angles. The red and green dashed boxes give examples of the obtained pictures from these cameras. (b) As the length L of the coated region (the blue rectangle on the fiber) decreases, the volume of the equilibrium barreled drop decreases. In this series of pictures, the coated length L and the dimensionless drop radius R_d/R_f are specified for each experiment. The red vertical arrow points the direction of the volume decrease. In this example, the coating layer of length L=7.6 mm provided the first clamshell droplet. A little longer layer, L=7.9 mm, resulted in a barreled drop. Therefore, the droplet volume corresponding to the layer length L=7.6 mm was reported as the critical volume for the barrel-to-clamshell transformation.

The process of drop formation was filmed by the high-resolution camera of the KRÜSS Drop shape analyzer and the USB camera (Neewer® digital microscope). These cameras were aimed at

different angles, from the top (USB camera) and from the side (KRÜSS camera). To produce a coating layer, the linear stage was set to move horizontally at constant speed of V = 3.15 mm/s.

When the stage moves, it pulls the liquid-filled tube with it and a liquid film gets deposited on the fiber. In this fiber coating process, the fiber remains stationary, but the tube moves. Thus, for an observer sitting on the tube, the fiber is withdrawn from the liquid-filled tube. As known from the Landau-Levich_Derjaguin (LLD) theory[13, 29-31], at the same withdrawal velocity V, the fibers of the same radius R_f and surface treatment (i.e. contact angle) should provide the same coating thickness h.

The stopper performance of the SMC Pollux Microstep Controller helped us to exclude the flow from the deposited film back to the feeding tube. The stage was programmed to displace the feeding tube to a prescribed distance at the chosen coating velocity V = 3.15 mm/s. Every time the stage stopped, the meniscus in the tube would keep slipping inside the tube. Doing so, it would always brake connection with the coated film. Therefore, as soon at the stage stopped, the liquid film gets disconnected from the tube and hence its further evolution in not influenced by the liquid in the tube. This way, changing the tube displacement L, we were able to control the length and hence the volume $2\pi R_f \cdot L \cdot h$ of the deposited liquid layer of thickness h.

This layer undergoes the Plateau-Rayleigh instability and forms a drop of the same volume $2\pi R_f \cdot L \cdot h$. For this problem, the receding contact angle was important. We measured the receding contact angle of grlycerol meniscus with the fiber to be 40°.

Starting from the longest coating distance L, the largest barrel was formed. Then the length of the coating film was decreased by $e = 300\mu m$ to obtain the film with a smaller volume $2\pi R_f(L -$

$e) \cdot h$. Then another liquid film shortened by $e = 300\mu m$ was formed and so on. Figures 3 (b-e) show different shapes of glycerol droplets formed by the described method on the same fiber.

As the coating length L decreased from 11.5 mm to 7.9 mm, the dimensionless drop size R_d/R_f decreased from 2.786 to 2.454. In this series of experiments, the clamshell drop was obtained for the first time when the length of liquid film was reduced to L=7.6 mm. Decreasing the film length L further resulted in clamshells. Therefore, the barreled drop shown in Fig. 3 (d) was reported as the critical barreled drop and the associated volume as the critical volume of a drop undergoing the barrel-to-clamshell transformation.

2.3. Materials

In these experiments, cylindrical glass tubes (Vitrocom) with the external diameters $2R_f = 250\ \mu m$ and $2R_f = 80\ \mu m$ the Basalt fibers (FibreCoat GmbH) of about 21 μm in diameter were used.

Compared with polymer fibers or metal wires, the glass tubes and basalt fibers offer smooth surfaces without any grooves or microdefects. To avoid the liquid evaporation during printing of small droplets, hexadecane (TCL) was used as the fluid.

To change the surface energy of the tube, chemical vapor deposition (CVD) of silanes was employed as detailed in Supporting material. Five types of silanes were applied and then the dynamic contact angles that hexadecane makes with the treated surfaces were measured using K100 Force Tensiometer(KRÜSS). The details of the contact angle analysis for basalt fibers can be found in Supporting material. Table 1 summarizes the results.

Table 1 Contact angle that hexadecane makes with the external surface of the tubes. The contact angles for the barreled droplets at the corresponding part of contact lines are given in parentheses (see examples in Fig. 5(d)).

tube O.D.[mm]	**silane**	**Advancing CA[°], hexadecane**	**Receding CA[°], hexadecane**	**Receding CA[°], glycerol**
0.25	2-[Methoxy(Polyethyleneoxy)6-9propyl]trimethoxysilane	22±2 (23±2, on the mobile part of contact line)	18±3(17±2, on the pinned part of contact line)	25±2
0.25	Methacryloxypropyltrimethoxysilane	29 ± 2(31 ± 1, on the mobile part of contact line)	19±3(19±2, on the pinned part of contact line)	38±1
0.25	(3-Glycidyloxypropyl)trimethoxysilane	-	-	40±3
0.25	UNTREATED TUBES	35 ± 2(33 ± 2, on the mobile part of contact line)	27±1(22±2, on the pinned part of contact line)	28±2
0.17	n-Octyldimethylchlorosilane	-	-	60±2
0.08	n-Octyldimethylchlorosilane	44 ± 2(46 ± 2, on the mobile part of contact line)	34±2(36±2, on the pinned part of contact line)	-
0.08	(Tridecafluoro-1,1,2,2-Tetrahtdrooctyl)trimethoxysilane	62±2	24±3	-

3. Results

3.1. Diagrams for barrel-clamshell transformations.

The results of all experiments are summarized in Fig. 4. The upper row in Figures 4 (a-e) illustrates the shapes of the smallest barreled drops that were obtained from small clamshells by printing droplets one after another on the same clamshell. Each of these images was obtained when

the clamshell transformed to the barreled droplet for the first time. Therefore, these barrels have the smallest volume. One could make them bigger by adding more droplets to these barrels.

The lower row in Figures 4 (a-e) illustrates the shapes of the smallest barreled drops obtained from the coating films. Decreasing the drop volume further, one would transform these barreled drops to clamshells.

Collecting all these results, one can build the drop transformation diagrams in Fig. 4 (f-g). The critical barreled drop that is about to form a clamshell is marked either as a blue cross or as a red hollow circle.

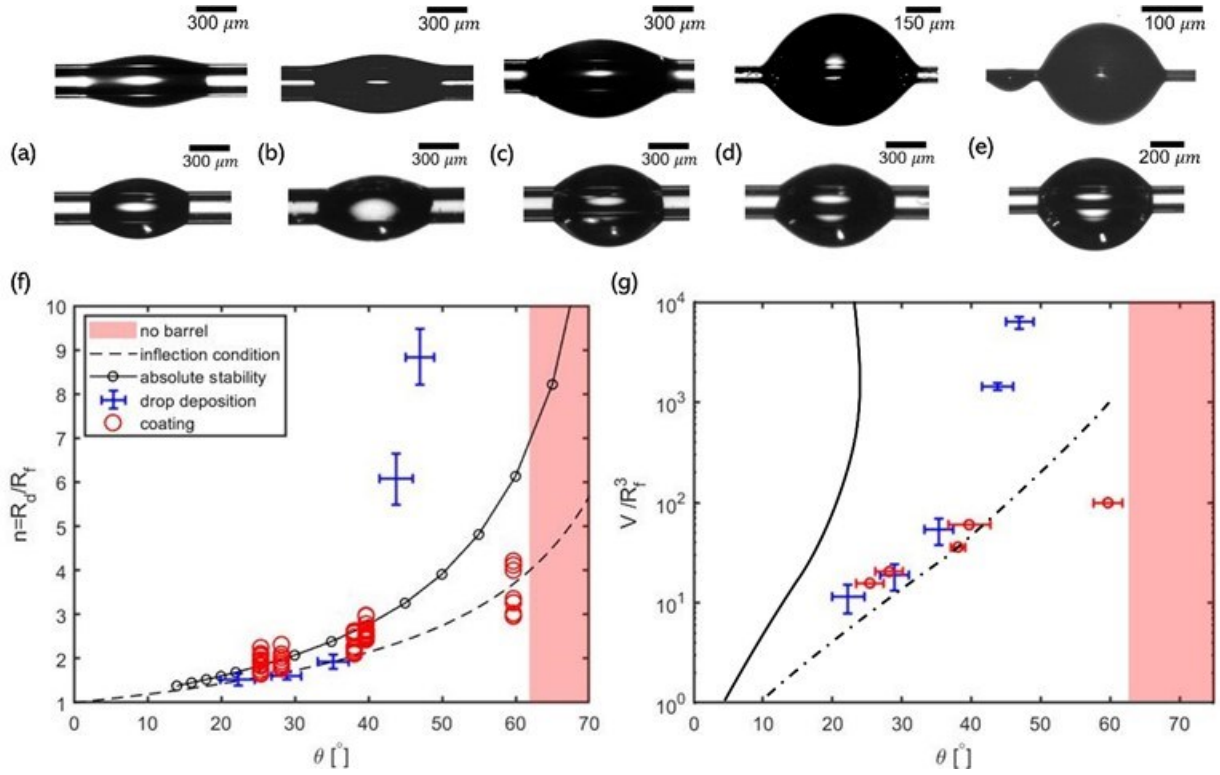

Fig. 4 (a)-(e). The upper row shows the critical barreled drops formed by printing liquid clamshells on different fibers offering different advancing & receding contact angles: (a) $\theta_{adv} = 22°$, $\theta_{rec} = 18°$. (b) $\theta_{adv} = 29°$, $\theta_{rec} = 19°$. (c) $\theta_{adv} = 35°$, $\theta_{rec} = 27°$, (d) $\theta_{adv} = 44°$, $\theta_{rec} = 34°$. (e) $\theta_{adv} = 47°$, $\theta_{rec} = 32°$. The lower row shows the barreled drops formed from the coating layer on the tubes offering different receding contact angles with glycerol: (a) $\theta_{rec} = 25°$, (b) $\theta_{rec} = 28°$, (c) $\theta_{rec} = 38°$, (d) $\theta_{rec} = 40°$, (e) $\theta_{rec} = 60°$. (f) The dimensionless drop radius versus contact angle diagram showing the transition boundary between the barreled and clamshell drops. The solid curve represents the absolute stability criterion[25], and the dashed curve

represents the inflection point condition[10]. The blue crosses formed by the error bars show the experimentally observed dimensionless radius n of the critical barreled drop formed by printing. The red circles represent barreled drops formed on the fiber by the coating method. (g) The dimensionless droplet volume versus contact angle diagram. The boundaries were numerically calculated in Ref[9] . The solid curve is the stability limit of the clamshell-to-barrel transition. The broken curve corresponds to the condition of equal absolute energy of clamshell and barreled droplets. The blue crosses are experimental data on drop printing. The red circles with the error bars were calculated using the unduloid solution as explained in Ref. [32] using the known contact angle and the ratio n . The lowest red circle was taken for each angle in (f).

In Figure 4 (g), we reproduced the diagram from Ref[9] and added new data to the diagram for cross-comparison. The solid curve determined by Mugele's group with the Surface Evolver shows the stability limit for clamshells; this boundary was validated by their electrowetting experiments. The broken curve was calculated from the condition of equal absolute energies for the clamshell and barreled droplets. This boundary was also confirmed by the electrowetting experiments. The model behind the calculated boundaries does not consider the contact angle hysteresis.

Comparing the data from the drop printing and film coating experiments, we observe that our datapoints deviate from the calculated boundaries. Our data suggest that for small contact angles ($< 40°$) and small hysteresis, the condition of equal absolute energies is a good criterion for identification of the clamshell-barrel transition. At the greater contact angles, the deviation from this criterion becomes significant. We, therefore, conducted a series of detailed visualization experiments to identify the causes for this disagreement.

3.2. Printed droplets

In this method, we grew a clamshell drop on a dry fiber by printing tiny droplets onto the same mother droplet. When the size of the growing clamshell reached its critical value, the clamshell spontaneously turned into a barreled drop (see Fig. 5). In the ideal case, to study this transition, one should ensure that no new droplets were added to the critical clamshell undergoing

transformation to the barrel. However, since the transition finished in a few milliseconds for small droplets or in hundreds of milliseconds for large droplets, it was not possible to stop the drop generator within this short time window. To see how the volume of the added drops influenced the transition, we estimated that total volume of added drops based on the known volume of a single produced droplet and the frequency of drop generator. In the small contact angle cases, the extra volume was about 1.9% of the volume of mother drop (i.e., Fig 5 (a)&(b)). For the large contact angle cases, the extra volume was less than 0.1% of the mother drop (i.e., Fig 5(c)). Thus, it is safe to assume that during clamshell-to-barrel transformation, the volume remained almost the same.

Since the drop was deposited on a dry fiber, the contact line moved forward over the dry surface and the drop formed advancing contact angle with the fiber. Using fibers with different surface energy, we observed different characteristic features of drop relaxation to its equilibrium configuration. We will discuss these phenomena for different ranges of contact angles.

Small advancing contact angles, $\boldsymbol{\theta_{adv} = 22°, 29°, 35°}$ **.** For droplets forming advancing contact angle smaller than 30°, the transformations from clamshells to barrels follow through very similar stages. Figures 5 (a) and (b) illustrate these stages using droplets that make the **22°** advancing contact angle with the tube. The yellow arrows point the direction of liquid flow during these stages of shape transition.

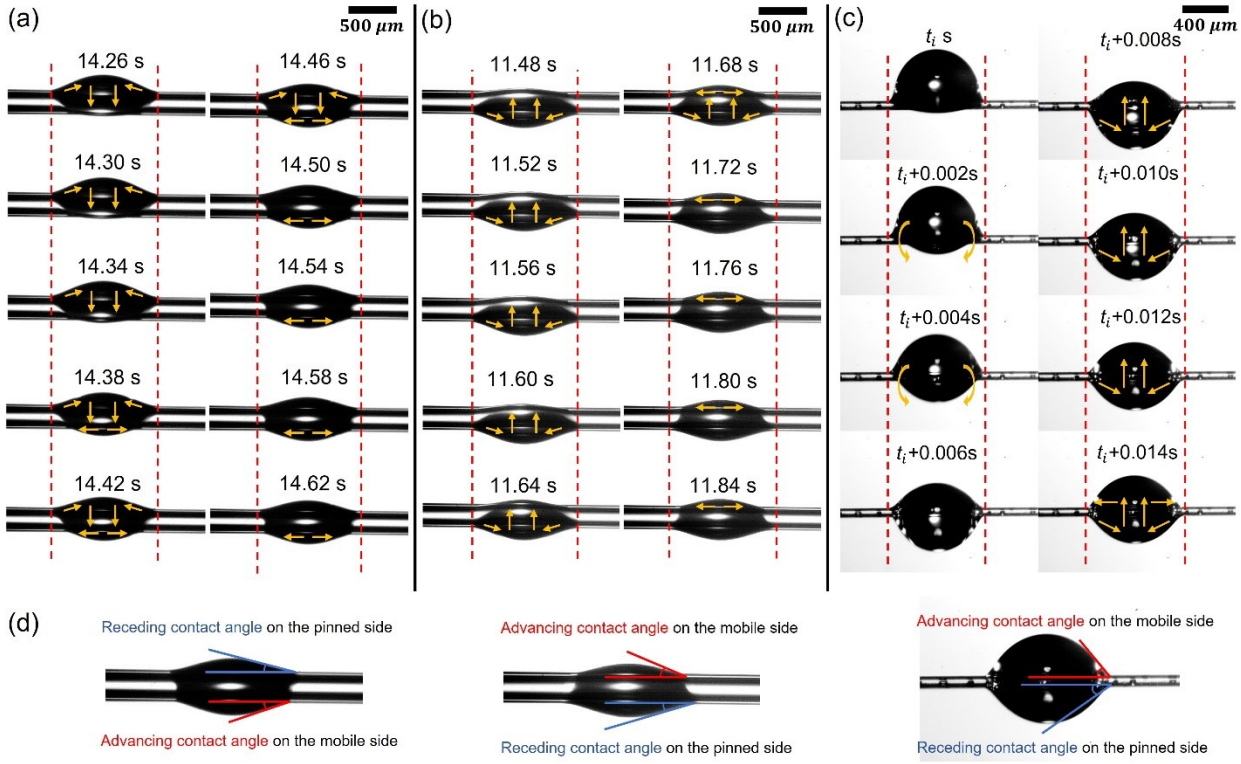

Fig. 5 (a) The main steps in transformation of a hexadecane drop making the 22° advancing contact angle with the tube of $2R_f$ =250 μm diameter. The clamshell drop was deposited from the top on this tube. The direction of drop movement has been inherited from the direction of falling droplets: in (a) it is from the top to the bottom. In (b) it is from the tube bottom where the droplets were printed from. The dashed lines mark the outermost boundary of the pinned contact lines. (c) The main steps in transformation of a hexadecane drop making the 44° advancing contact angle with the tube of $2R_f = 80\ \mu m$ diameter. The clamshell of critical volume has been formed at time moment t_i, $t_i \approx 40$ seconds. In contrast to figures (a) and (b), where the drop spreads over the initially dry part and the liquid is pushed from the back of the clamshell by the capillary pressure, the drop in (c) first rolled from the top to the bottom of the tube (within the time span from t_i to t_i +0.006s) making the bigger bulge hanging down. After formation of a non-symmetric barrel, the drop relaxed to its equilibrium axisymmetric barreled shape by moving liquid from this large bulge

at the bottom to the smaller bulge at the top. (d) The advancing and receding contact angles on the barreled drop right after the transitions in (a)-(c). The angle at the pinned contact line during the transition is marked as the receding contact angle while the angle on at the mobile contact line is marked as the advancing contact angle.

In Fig. 5(a), the clamshell drop was deposited from above on the top surface of the tube. The arrows in Fig. 5 show the velocity directions of fluid particles. As soon as the critical clamshell volume has been reached (14.26 s), the fluid starts to move from the clamshell sides to the dry bottom surface of the tube (14.26 s-14.34 s). At the time moment, when the advancing parts of the contact line merge together at the bottom of the tube (14.34s), a barreled droplet formed. At this moment, a single contact line broke onto two contact lines that encircled the tube from the left and right sides of the barreled droplet.

After nucleation of a barreled droplet, the lower part of the barrel started spreading along the bottom side of the tube while the liquid inside the bulge on the top side of the tube flip the flow direction toward the droplet center (14.28 s-14.46 s). The red dashed line shows that during the clamshell-barrel transition, the upper part of the contact line remained pinned at the original position; however, the lower part of the contact line on the tube bottom significantly extended.

In the experiment shown in Fig. 5(b), we printed drops on the sidewall of the tube. In this case, when the clamshell grew further, it moved to the bottom of the tube. In the sequence of pictures shown in Fig. 5(b), we started from 11.48 s when the clamshell drop has already been formed at the tube bottom. To illustrate the clamshell-to-barrel transition, we tracked the droplet movement after that moment on. The phenomenon was similar to that shown in Fig. 5(a) but the flow occurred in the direction opposite to the direction of acceleration due to gravity, proving that gravity plays no role in this transition.

For the 29° contact angles, the transformation of clamshell to barrel followed similar steps but happened faster. For the 29° angle, it happened within about 0.34 s for , which is 0.06 s faster than in the case of 22° contact angle. Thus, the greater the angle, the faster the clamshell-barrel transition happens.

Medium advancing contact angles, $\boldsymbol{\theta_{adv} = 35°, 44° \text{ \& } 47°}$ **.** According to the drop transformation diagram shown in Fig. 1, for contact angles larger than 40°, we expected much greater critical volume for the clamshell-barrel transition. To check this prediction and reduce the influence of gravity, the 80 μm diameter capillary tubes were used. Surprisingly, the size of the barreled drop at its critical volume was much larger than that predicted by the accepted drop transformation diagram[11]. Figure 5 (c) shows the transformation steps from clamshells - to barrels. A different transition mode was observed. As the clamshell reached its critical volume, it spontaneously rolled over the tube to form a bigger bulge at the bottom side of this tube. This happens very fast, within the time span of 0.006s. Then the liquid moved against gravity from the larger bulge at the bottom to the top feeding a smaller bulge.

During transformation, the contact line remained pinned at the outermost boundary of the liquid body indicated by the red dashed line. The transformation from clamshell to barrel took only 0.014 s, which is one order of magnitude faster than the previous ones. Similar features can be observed when the droplets are deposited on the tubes of the $2R_f$ =250 μm diameter with which hexadecane made the 35° advancing contact angle, and on basalt fibers of the $2R_f$ =42 μm diameter and the 47° advancing contact angle, see the details in Supporting material.

Large advancing contact angle, $\boldsymbol{\theta_{adv} = 62°}$. Theoretically, the barreled drops could be formed at large contact angles $\theta_{adv} > 60°$. However, all our attempts to make these drops failed. Moving

the printhead along the 80 μm diameter tube, we formed multiple clamshell drops. No transition to a barreled drop occurred. Figure 6 (a) and (b) were taken 5 minutes after the drop printing was stopped. As shown in Fig. 6(a), relatively large clamshell drops can stably sit on the top of the tube surface. No liquid bridges that would connect adjacent clamshells on the top and on the bottom surface of the tube were found, implying that the bottom side of the clamshell drop was completely dry. To further prove that the bottom side of a clamshell drop was dry, we printed more drops on the top of the clamshell, as shown in the magnified Fig. 6(b). The fact that these tiny droplets can stay on the surface not being absorbed by the adjacent big clamshells supports the bridge-free scenario.

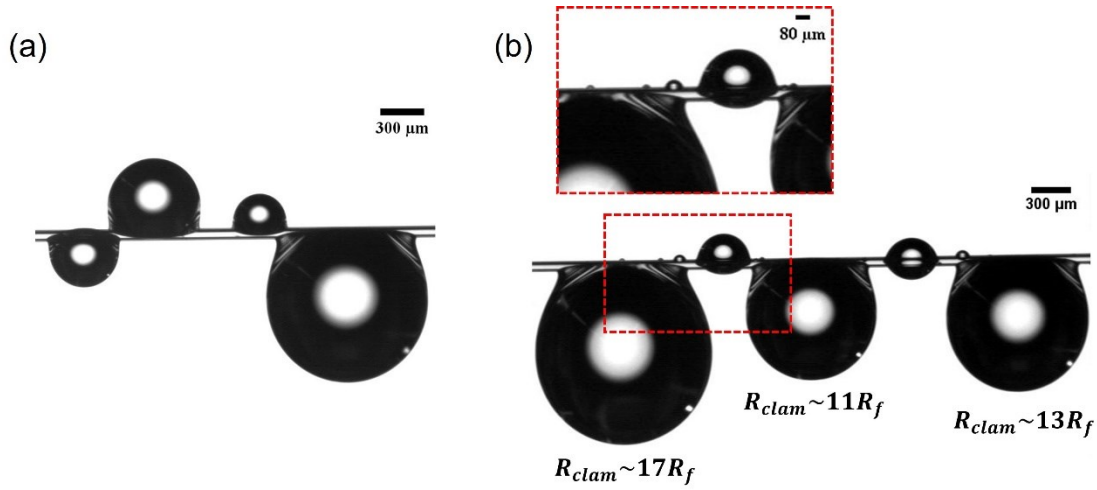

Fig. 6 (a) Behavior of hexadecane droplets making 62° advancing contact angles with the tubes. Only clamshells were observed. (b) When tiny drops were purposely printed between clamshells, they remained locked in place. These experiments suggest that the smaller drops were not connected to the larger clamshells.

3.3. Formation of droplets from liquid films

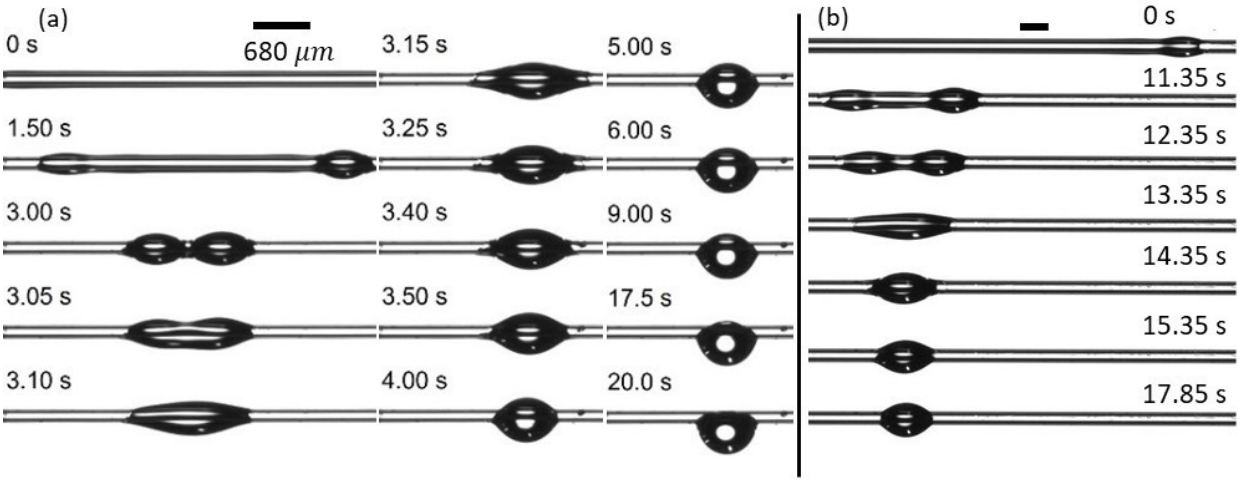

Fig. 7. The main steps illustrating drop formation from liquid films. (a) Experiment with glycerol that makes 60° receding contact angle with the tube of $2R_f = 170\ \mu m$ diameter. At the first time moment (0 s), a thin film of glycerol was deposited on a tube of. Due to the Plateau-Rayleigh instability, the film collapsed in a dumbbell (1.50 s). The dumbbell coalesced (3.00 s) to form a single barreled drop (3.10 s). The drop kept gathering liquid from the film (3.15 s-3.50 s) until the film shrank. Starting from the frame taken at 3.50 s, no film could be seen, but the liquid flows from one side of the drop to the other and the contact line visibly deforms (3.50 s-15.5 s). Finally, the barreled drop turned into a clamshell (20.0 s). (b) Experiment with glycerol that makes 40° receding contact angle with the tube of $2R_f = 250\ \mu m$ diameter. Due to the Plateau-Rayleigh instability, a series of barreled drop were formed. In frame (0 s), one can see only a single drop. In frame (11.35 s), the second drop appeared and scenario of formation of a single barrel repeated that in figure (a). Once the barreled droplet has formed (14.35 s), only small deformations of the contact line were detected (14.35 s-17.85 s) and the final barreled drop (17.85 s) formed almost mirror-symmetric contact lines at its left and right ends.

The fiber was coated with a thin film of glycerol, Fig. 7 (a)-(b). The transition from a barrel-like drop to a clamshell drop was observed either (i) when the film thickness is very small so that the amount of liquid was insufficient to form a barreled drop after the film breakup, or (ii) when the contact angle that glycerol made with a fiber was large. Figures 7 (a)-(b) illustrate the dynamics of drop formation. In contrast to the scenario of drop formation by printing, Fig. 5 (a)-(c), the drop is formed from the liquid film and when it forms, it keeps contracting; therefore, only receding

contact angle is important for this scenario. We noticed that all liquid initially collected in the coating films will move in the drop and no other visible liquid residues remained on the tube.

Figure 7 (a) illustrates the case of large 60° receding contact angle when the final droplet has a clamshell shape. The film first formed a dumbbell (1.5 s in Fig. 7 (a)) due to the Plateau-Rayleigh instability[27, 28, 33], and then two sides of the dumbbell coalesce to form a single barreled drop. This barreled drop later transforms into a clamshell. Figure 7 (b) illustrates the case of small 40° receding contact angle where the barreled drop persists and collects all the liquid from the coating film.

4. Summary of results and discussion

Drops on glass tubes and fibers making advancing contact angles of 22°, 29°, 35°, 44°, 47° allowed us to investigate characteristic features of clamshell-barrel transition.

We call a barreled drop critical when that drop has been formed from a liquid clamshell for the first time. This drop has the minimum volume required for a clamshell drop to transit to a barreled drop. A summary panel, Figure 4, illustrates the shapes of critical barreled drops that make different contact angles with the tubes/fibers. When the advancing contact angle increases, the maximum diameter $2R_d$ of the critical barreled drop relative to the fiber diameter $2R_f$ increases as well.

To investigate the influence of the contact angle on the clamshell-barrel transition, we calculated the critical ratio[20] $n = R_d/R_f$ for all critical barreled drops. To include slightly asymmetric barreled drop, we redefined the barrel radius as

$$R_d = \frac{maximun\ distance\ between\ bulges}{2}$$

and the new ratio $n = R_d/R_f$ was shown in Fig. 4(e).

The experimental results are added to the existing diagram. In Figure 4(f) (see also Fig. S7 in Supporting material), the relation between the critical ratio n and the measured advancing contact angles is shown by the blue crosses, with the error bars calculated as the half-value width of their standard deviations measured in experiments. In parallel, we plot the dimensionless volume, V/R_f^3 for the first barreled drop versus advancing contact angle, Figure 4(g). The new results show significant deviation from the theoretical prediction and electrowetting experiments.

The obtained diagram has three regions. In one region, large droplets could form only stable barrels. In the other region, small droplets could form only clamshells. These two regions are separated by a region where one could form barrels or clamshells, i.e. both configurations may have the same energies and could be stable. And one configuration could be spontaneously transformed into the other. In other words, the barrel-clamshell transformations can occur anywhere within this bistability region. The bistability region given in Ref.[9] is very large and all our datapoints fall within this region. Therefore, predictions based on the model[9] with a single contact angle give an upper estimate for volumes of barreled droplets and lower estimate for volumes of clamshells. Hence, the existing model is very conservative and provides a great safety factor for an engineer. On one hand it is good, on the other hand, one questions: "Where the actual transformation happens and how it would depend on the experimental conditions?" Our experimental protocols are motivated by the aerosol filtration and fiber coating applications where the experimental conditions are far from those modeled by the electrowetting experiments.

These arguments drew our attention to the role of contact angle hysteresis in the drop transformations. We mentioned earlier that all barreled drops obtained from printed clamshells

were always slightly asymmetric; this asymmetry has been observed earlier and reported in Refs. [6, 8]. In the recent publication [8], the authors suggested that the nearly asymmetric barreled drop can be explained by its sagging under own weight. Although the explanation was confirmed by experiments on the polyalphaolefin (PAO4) droplets deposited on fibers with the radii of 128, 221, and 600 μm, we cannot completely agree with this explanation: we showed that clamshells are able to move against gravity to form barrels. Table S3 also suggests that the Bond numbers in our experiments are very small and hence gravity should not play any significant role.

We, therefore, looked more carefully at the role of contact angle hysteresis. As seen in Fig. 5, during the clamshell-barrel transformation, the outermost part of the contact line of original clamshell remained pinned at the same initial boundary. We investigated the contact angles at this pinned contact line and at the contact line formed by the other part of barreled drop, the details are given in **Supporting material**.

In Table 1, we collected all the measured contact angles formed at the pinned and mobile parts of the contact line. Comparison with the contact angle values measured by the K100 Force Tensiometer and the image analysis data allowed us to conclude that the contact angles formed at the mobile part of the contact line were always closer to the advancing contact angle values, while the contact angles at the pinned contact line are close to the receding contact angles. We observed a similar trend for droplets deposited on the ribbon-like fibers[34] where this effect was more pronounced.

For the contact line depinning, the clamshell must adjust its shape to deform the liquid wedge at the pinned contact line: the liquid wedge must change its angle from advancing to receding contact angle. During this transformation, that part of the contact line remains pinned, and the angle gradually changes as the liquid moves from the wedge toward the droplet center as shown

in Fig. 5. In the final barreled droplet this angle is very close to the receding contact angle suggesting that that part of the contact line might has been depinned and displaced just a little. Our camera resolution was not able to detect this small movement. We expect that the final configuration of the barreled drop should be symmetrical with equilibrium contact angle between receding and advancing values.

These observations confirm that the contact angle hysteresis contributes to the drop asymmetry and supports our hypothesis explaining why we see deviations from theoretical predictions. The theoretical boundaries in the clamshell-barrel diagrams in Fig. 4 (f)-(g) are calculated neglecting the contact angle hysteresis and hence were not able to distinguish different scenarios of contact line movements. In the electrowetting experiments, the contact angle hysteresis was, most likely, minute and hence the model with a single contact angle was appropriate for explanation of the drop behavior.

5. Conclusion

Summary of key findings. We asked: "DOES THE CONTACT ANGLE HYSTERESIS CONTROL THE DROPLET SHAPE ON CYLINDRICAL FIBER?" To answer this question, we experimentally studied the transformations between the clamshell and barreled drops. Fibers with different contact angles have been used. It is shown that the critical conditions for this transformation are deviated from all existing theoretical predictions. In experiments on the droplet-fiber pairs with small ($< 40°$) advancing contact angles and small contact angle hysteresis, the datapoints lie closer to the theoretical boundary. In experiments on the droplet-fiber pairs offering advancing contact angle greater than 40°, to turn into a barrel, the clamshell drop was shown to require a volume greater than the theoretically predicted one. In contrast to the theoretical

prediction, we never observed the clamshell-barrel transformation when the advancing contact angle was increased above 60°. The results of all experiments are summarized in Fig.4.

Highlights of the hypothesis, new concepts, and innovations. Using two methods of drop formation, by printing droplets on the fiber and by forming droplets from coating films taking advantage of the Plateau-Raleigh instability of these films, we were able to reveal new important features of this transformation. We hypothesized that the contact angle hysteresis is responsible for the clamshell-barrel shape transformation of droplets. To check this hypothesis, the contact angles on the mirror-symmetric but not axisymmetric drops were studied in detail. The barreled droplets formed from the coating films appeared axisymmetric and the data on the drop volume versus contact angle followed theoretical predictions based only on receding contact angle[9]. The barreled droplets formed by printing appeared mirror-symmetric but not axisymmetric. When one droplet bulge forms receding contact angle with the fiber, the other forms advancing contact angle. The corresponding data points for the clamshell-barrel transformation deviate significantly from the theory based on a single contact angle. We suggest that the contact angle hysteresis is an important factor significantly influencing the transformation of clamshells to barreled droplets. Thus, the drop volume, fiber radius, advancing contact angle θ_{adv} and receding contact angle θ_{rec} are the main parameters controlling the droplet shape.

Future developments and engineering and materials science applications. The obtained diagrams and experimental protocols could be used in many engineering applications dealing with filtration[1, 5] and printing[35, 36] as well in many biological applications [15, 37-40]. For example, hovering hawkmoths with long proboscises benefit from pulling out a nectar film on its surface[40]. When the insect withdraws its proboscis from the flower, this film could be sipped up during flight. Therefore,

adhesion of the film followed by formation of firmly attached droplets[39] is critical for the insects with a high energy demand for its flight. We expect that this work will draw attention of biologists evaluating the evolutionary pathway of proboscis developments[41]; the contact angle hysteresis could be an important character separating hawkmoths from butterflies and other moths. The paper offers a new insight on the classical problem of morphological transitions of droplet configurations on curved substrates and significantly expands the library of experimental data. The importance of contact angle hysteresis in these transitions has not been appreciated yet and we hope that the obtained results will pave a way to develop new approaches and theories helping to design new advanced materials.

Acknowledgements

This work was partially supported by National Science Foundation award IOS- 2042937 and the SC EPSCoR/IDeA Program under NSF Award No. OIA-1655740. The views, perspectives, and content do not necessarily represent the official views of the SC EPSCoR/IDeA Program northose of the NSF.

Figure captions and Tables

Fig.1. The diagram of the clamshell-barrel transformations numerically obtained in Ref.[9]. The inserts illustrate the shapes of barreled drop and clamshell drops. The black solid line is the boundary when no clamshell droplets could be formed, and the red solid line is the boundary when no barreled droplets could be formed. The broken line indicates the condition of equal absolute energy of the barreled and clamshell droplets.

Fig. 2 Schematic of the drop printing setup that consists of three main parts. (i) A microdrop generator controlling the drop size. The drop placement is controlled by a 3D manipulator holding the microdrop generator. (ii) A U-shaped holder with the fiber. The fiber axis is taken as the x-axis of the system of coordinates of manipulator as shown in the picture. (iii) A high speed-motion camera and a diffused light source. The insert shows the actual experimental setup.

Fig. 3 (a) Schematic of the experimental setup for fiber coating experiments. The fiber is fixed at one end on a holder and its other end is immersed in a liquid-filled tube placed on a linear stage.

The fiber gets coated when the stage is set to move at a given velocity. Two cameras film the drop formation process from different angles. The red and green dashed boxes give examples of the obtained pictures from these cameras. (b) As the length *L* of the coated region (the blue rectangle on the fiber) decreases, the volume of the equilibrium barreled drop decreases. In this series of pictures, the coated length L and the dimensionless drop radius R_d /R_f are specified for each experiment. The red vertical arrow points the direction of the volume decrease. In this example, the coating layer of length L=7.6 mm provided the first clamshell droplet. A little longer layer, L=7.9 mm, resulted in a barreled drop. Therefore, the droplet volume corresponding to the layer length L=7.6 mm was reported as the critical volume for the barrel-to-clamshell transformationFig. 4 (a) Clamshells are the only shapes observed when the hexadecane droplets where printed of the tubes making 62° advancing contact angle with it. (b) Some tiny drops were purposely placed on the bottom side of the clamshell drop, and none of them disappeared later. This suggests that the drops were not connected to the larger clamshells.

Fig. 4 (a)-(e). The upper row shows the critical barreled drops formed by printing liquid clamshells on different fibers offering different advancing & receding contact angles: (a) $\theta_{adv} = 22°$, $\theta_{rec} = 18°$. (b) $\theta_{adv} = 29°$, $\theta_{rec} = 19°$. (c) $\theta_{adv} = 35°$, $\theta_{rec} = 27°$, (d) $\theta_{adv} = 44°$, $\theta_{rec} = 34°$. (e) $\theta_{adv} = 47°$, $\theta_{rec} = 32°$. The lower row shows the barreled drops formed from the coating layer on the tubes offering different receding contact angles with glycerol: (a) $\theta_{rec} = 25°$, (b) $\theta_{rec} = 28°$, (c) $\theta_{rec} = 38°$, (d) $\theta_{rec} = 40°$, (e) $\theta_{rec} = 60°$. (f) The dimensionless drop radius versus contact angle diagram showing the transition boundary between the barreled and clamshell drops. The solid curve represents the absolute stability criterion[25], and the dashed curve represents the inflection point condition[10]. The blue crosses formed by the error bars show the experimentally observed dimensionless radius n of the critical barreled drop formed by printing. The red circles represent barreled drops formed on the fiber by the coating method. (g) The dimensionless droplet volume versus contact angle diagram. The boundaries were numerically calculated in Ref[9] . The solid curve is the stability limit of the clamshell-to-barrel transition. The broken curve corresponds to the condition of equal absolute energy of clamshell and barreled droplets. The blue crosses are experimental data on drop printing. The red circles with the error bars were calculated using the unduloid solution as explained in Ref. [32] using the known contact angle and the ratio n . The lowest red circle was taken for each angle in (f).

Fig. 5 (a) The main steps in transformation of a hexadecane drop making the 22° advancing contact angle with the tube of $2R_f$ =250 μm diameter. The clamshell drop was deposited from the top on this tube. The direction of drop movement has been inherited from the direction of falling droplets: in (a) it is from the top to the bottom. In (b) it is from the tube bottom where the droplets were printed from. The dashed lines mark the outermost boundary of the pinned contact lines. (c) The main steps in transformation of a hexadecane drop making the 44° advancing contact angle with the tube of $2R_f = 80\ \mu m$ diameter. The clamshell of critical volume has been formed at time moment t_i, $t_i \approx 40$ seconds. In contrast to figures (a) and (b), where the drop spreads over the initially dry part and the liquid is pushed from the back of the clamshell by the capillary pressure, the drop in (c) first rolled from the top to the bottom of the tube (within the time span from t_i to t_i +0.006s) making the bigger bulge hanging down. After formation of a non-symmetric barrel, the drop relaxed to its equilibrium axisymmetric barreled shape by moving liquid from this large bulge at the bottom to the smaller bulge at the top. (d) The advancing and receding contact angles on the

barreled drop right after the transitions in (a)-(c). The angle at the pinned contact line during the transition is marked as the receding contact angle while the angle on at the mobile contact line is marked as the advancing contact angle.

Fig. 6 (a) Behavior of hexadecane droplets making 62° advancing contact angles with the tubes. Only clamshells were observed. (b) When tiny drops were purposely printed between clamshells, they remained locked in place. These experiments suggest that the smaller drops were not connected to the larger clamshells.

Fig. 7. The main steps illustrating drop formation from liquid films. (a) Experiment with glycerol that makes 60° receding contact angle with the tube of $2R_f = 170\ \mu m$ diameter. At the first time moment (0 s), a thin film of glycerol was deposited on a tube of. Due to the Plateau-Rayleigh instability, the film collapsed in a dumbbell (1.50 s). The dumbbell coalesced (3.00 s) to form a single barreled drop (3.10 s). The drop kept gathering liquid from the film (3.15 s-3.50 s) until the film shrank. Starting from the frame taken at 3.50 s, no film could be seen, but the liquid flows from one side of the drop to the other and the contact line visibly deforms (3.50 s-15.5 s). Finally, the barreled drop turned into a clamshell (20.0 s). (b) Experiment with glycerol that makes 40° receding contact angle with the tube of $2R_f = 250\ \mu m$ diameter. Due to the Plateau-Rayleigh instability, a series of barreled drop were formed. In frame (0 s), one can see only a single drop. In frame (11.35 s), the second drop appeared and scenario of formation of a single barrel repeated that in figure (a). Once the barreled droplet has formed (14.35 s), only small deformations of the contact line were detected (14.35 s-17.85 s) and the final barreled drop (17.85 s) formed almost mirror-symmetric contact lines at its left and right ends.

Table 2 Contact angle that hexadecane makes with the external surface of the tubes. The contact angles for the barreled droplets at the corresponding part of contact lines are given in parentheses (see examples in Fig. 5(d)).

tube O.D.[mm]	**silane**	**Advancing CA[°], hexadecane**	**Receding CA[°], hexadecane**	**Receding CA[°], glycerol**
0.25	2-[Methoxy(Polyethyleneoxy)6-9propyl]trimethoxysilane	22 ± 2 (23 ± 2, on the mobile part of contact line)	18 ± 3(17 ± 2, on the pinned part of contact line)	25 ± 2
0.25	Methacryloxypropyltrimethoxysilane	29 ± 2(31 ± 1, on the mobile part of contact line)	19 ± 3(19 ± 2, on the pinned part of contact line)	38 ± 1
0.25	(3-Glycidyloxypropyl)trimethoxysilane	-	-	40 ± 3
0.25	UNTREATED TUBES	35 ± 2(33 ± 2, on the mobile	27 ± 1(22 ± 2, on the pinned	28 ± 2

		part of contact line)	part of contact line)	
0.17	n-Octyldimethylchlorosilane	-	-	60±2
0.08	n-Octyldimethylchlorosilane	44 ± 2(46 ± 2, on the mobile part of contact line)	34±2(36±2, on the pinned part of contact line)	-
0.08	(Tridecafluoro-1,1,2,2-Tetrahtdrooctyl)trimethoxysilane	62±2	24±3	-

References

1. Brown, P.; Cox, C., *Fibrous Filter Media*. Woodhead Publishing: 2017.
2. Adam, N. K., Detergent Action and its Relation to Wetting and Emulsification. *Journal of the Society of Dyers and Colourists* **1937,** *53* (4), 121-129.
3. Cassie, A. B. D., Physics and textiles. *Reports on Progress in Physics* **1945,** *10*, 141-171.
4. Miller, B., The wetting of fibers. In *Surface characteristics of fibers and textiles*, Schick, M. J., Ed. Marcel Dekker: New York, 1977; Vol. 2, pp 417-445.
5. Duprat, C., Moisture in Textiles. *Annual Review of Fluid Mechanics* **2022,** *54*, 443-467.
6. Chou, T. H.; Hong, S. J.; Liang, Y. E.; Tsao, H. K.; Sheng, Y. J., Equilibrium Phase Diagram of Drop-on-Fiber: Coexistent States and Gravity Effect. *Langmuir* **2011,** *27* (7), 3685-3692.
7. Xu, C. W.; Lu, Z. Y.; Li, L. R., Surface Evolver Simulation of Droplet Wetting Morphologies on Fiber Without Gravity. *Frontiers in Energy Research* **2022,** *9*.
8. Gupta, A.; Konicek, A. R.; King, M. A.; Iqtidar, A.; Yeganeh, M. S.; Stone, H. A., Effect of gravity on the shape of a droplet on a fiber: Nearly axisymmetric profiles with experimental validation. *Physical Review Fluids* **2021,** *6* (6).
9. Eral, H. B.; de Ruiter, J.; de Ruiter, R.; Oh, J. M.; Semprebon, C.; Brinkmann, M.; Mugele, F., Drops on functional fibers: from barrels to clamshells and back. *Soft Matter* **2011,** *7* (11), 5138-5143.
10. McHale, G.; auml; b, N. A.; Newton, M. I.; Rowan, S. M., Wetting of a High-Energy Fiber Surface. *J Colloid Interface Sci* **1997,** *186* (2), 453-61.
11. McHale, G.; Newton, M. I., Global geometry and the equilibrium shapes of liquid drops on fibers. *Colloids and Surfaces A: Physicochemical and Engineering Aspects* **2002,** *206*, 79-86.
12. McHale, G.; Newton, M. I.; Carroll, B. J., The shape and stability of small liquid drops on fibers. *Oil & Gas Science and Technology-Revue De L Institut Francais Du Petrole* **2001,** *56* (1), 47-54.
13. Quere, D., Fluid coating on a fiber. *Annual Review of Fluid Mechanics* **1999,** *31*, 347-384.
14. Opell, B. D., Water harvesting during orb web recycling. *Journal of Arachnology* **2020,** *48* (3), 278-283.

15. Opell, B. D.; Jain, D.; Dhinojwala, A.; Blackledge, T. A., Tuning orb spider glycoprotein glue performance to habitat humidity. *Journal of Experimental Biology* **2018,** *221* (6).
16. Stellwagen, S. D.; Opell, B. D.; Clouse, M. E., The impact of UVB radiation on the glycoprotein glue of orb-weaving spider capture thread. *Journal of Experimental Biology* **2015,** *218* (17), 2675-2684.
17. Seeber, M.; Zdyrko, B.; Burtovvy, R.; Andrukh, T.; Tsai, C. C.; Owens, J. R.; Kornev, K. G.; Luzinov, I., Surface grafting of thermoresponsive microgel nanoparticles. *Soft Matter* **2011,** *7* (21), 9962-9971.
18. Lu, C. R.; Wang, J.; Lu, X.; Zheng, T.; Liu, Y. Y.; Wang, X. D.; Zhang, D. X.; Seveno, D., Wettability and Interfacial Properties of Carbon Fiber and Poly(ether ether ketone) Fiber Hybrid Composite. *Acs Applied Materials & Interfaces* **2019,** *11* (34), 31520-31531.
19. Carroll, B. J., The Accurate Measurement of Contact-Angle, Phase Contact Areas, Drop Volume, and Laplace Excess Pressure in Drop-on-Fiber Systems. *Journal of Colloid and Interface Science* **1976,** *57* (3), 488-495.
20. Carroll, B. J., Equilibrium conformations of liquid drops on thin cylinders under forces of capillarity. A theory for the roll-up process. *Langmuir* **1986,** *2* (2), 248-250.
21. Sun, X. H.; Zhang, W. W.; Lee, H. J.; Michielsen, S., Equilibrium clamshell drops on conical surfaces: effect of curvature and gravity. *Colloid Surf. A-Physicochem. Eng. Asp.* **2019,** *572*, 203-210.
22. McHale, G.; Newton, M. I.; Carroll, B. J., The shape and stability of small liquid drops on fibers. *Oil Gas Sci Technol* **2001,** *56* (1), 47-54.
23. Rebouillat, S.; Letellier, B.; Steffenino, B., Wettability of single fibres – beyond the contact angle approach. *Int. J. Adhes. Adhes.* **1999,** *19* (4), 303-314.
24. Carroll, B. J.; Lucassen, J., Effect of surface dynamics on the process of droplet formation from supported and free liquid cylinders. *Journal of the Chemical Society, Faraday Transactions 1: Physical Chemistry in Condensed Phases* **1974,** *70* (0), 1228-1239.
25. McHale, G.; Newton, M. I., Global geometry and the equilibrium shapes of liquid drops on fibers. *Colloids and Surfaces A: Physicochemical and Engineering Aspects* **2002,** *206* (1-3), 79-86.
26. Brakke, K. A., The Surface Evolver. *Experimental Mathematics* **1992,** *1* (2), 141-165.
27. Plateau, J., Experimental and theoretical researches on the figures on equilibrium of a liquid mass withdrawn from the action of gravity. In *Annual Report of the Board of Regents of the Smithsonian Institution* Smithsonian Institution: Washington, DC, 1863; pp 207–285.
28. Rayleigh, L., On the capillary phenomena of jets. *Proc. R. Soc. Lond. A* **1879,** *29*, 71-97.
29. Landau, L. D.; Levich, V. G., Dragging of a liquid by a moving plate. *Acta Physicochim. URSS* **1942,** *17*, 42.
30. Derjaguin, B. V., Thickness of the liquid film adhering to a moving thread. *Doklady Akademii Nauk Sssr* **1943,** *39*, 11.
31. Zhang, Z.; Salamatin, A.; Peng, F.; Kornev, K. G., Dip coating of cylinders with Newtonian fluids. *Journal of Colloid and Interface Science* **2022,** *607*, 502-513.
32. Sun, Y. M.; Ma, J. X.; Peng, F.; Kornev, K. G., Making droplets from highly viscous liquids by pushing a wire through a tube. *Physics of Fluids* **2022,** *34* (3).

33. Haefner, S.; Benzaquen, M.; Baumchen, O.; Salez, T.; Peters, R.; McGraw, J. D.; Jacobs, K.; Raphael, E.; Dalnoki-Veress, K., Influence of slip on the Plateau-Rayleigh instability on a fibre. *Nat Commun* **2015,** *6*, 7409.
34. Zhang, C. Q.; Kornev, K. G., Morphological transitions of drop configurations on ribbon-like fibers. *Surface Innovations* **2017,** *5* (4), 194-202.
35. Park, H.; Carr, W. W.; Ok, H.; Park, S., Image quality of inkjet printing on polyester fabrics. *Text. Res. J.* **2006,** *76* (9), 720-728.
36. Raut, N. C.; Al-Shamery, K., Inkjet printing metals on flexible materials for plastic and paper electronics. *Journal of Materials Chemistry C* **2018,** *6* (7), 1618-1641.
37. Zarzar, L. D.; Sresht, V.; Sletten, E. M.; Kalow, J. A.; Blankschtein, D.; Swager, T. M., Dynamically reconfigurable complex emulsions via tunable interfacial tensions. . *Nature* **2015,** *518*, 520–524
38. Shin, Y.; Brangwynne, C. P., Liquid phase condensation in cell physiology and disease. *Science* **2017,** *357*, 1253.
39. Zhang, C. Q.; Beard, C. E.; Adler, P. H.; Kornev, K. G., Effect of curvature on wetting and dewetting of proboscises of butterflies and moths. *Royal Society Open Science* **2018,** *5* (1).
40. Kornev , K. G.; Adler, P. H., Physical determinants of fluid feeding in insects. In *Insect mouthparts- form, function, development and performance*, Krenn, H., Ed. Springer: New York, 2019; pp 263-314.
41. Kawahara, A. Y. Molecular phylogenetic analysis of the hawkmoths (Lepidoptera: Bombycoidea: Sphingidae) and the evolution of the sphingid proboscis. . University of Maryland, College Park., University of Maryland, College Park., 2007.
42. Zhang, Z.; Peng, F.; Kornev, K. G., The Thickness and Structure of Dip-Coated Polymer Films in the Liquid and Solid States. *Micromachines* **2022,** *13* (7), 982.
43. Alimov, M. M.; Kornev, K. G., Meniscus on a shaped fibre: singularities and hodograph formulation. *Proceedings of the Royal Society a-Mathematical Physical and Engineering Sciences* **2014,** *470* (2168).

DOES THE CONTACT ANGLE HYSTERESIS CONTROL THE DROPLET SHAPES ON CYLINDRICAL FIBERS?

Yueming Sun and Konstantin G. Kornev

515 Calhoun Drive, 161 Sirrine Hall, Deptartment of Materials Science and Engineering, Clemson University, SC 29634, USA

Supporting material

S1. Calibration of the microdrop dispenser and method of drop deposition

The microdrop dispenser produces single micro drops by applying a pulsed voltage to the piezo actuator inside the printing nozzle. The applied voltage and pulse length are adjusted to generate microdroplets of the same diameter. The stroboscope supplied with the microdrop dispenser can be used to ensure that only a single drop per pulse is printed from the nozzle. Filming the drop formation at 50,000 fps, we estimated that a single drop is formed every 4950 μs. To evaluate the drop volume, we analyzed the images using ImageJ (NIH) and obtained the area A of each micro drop from the frames, then the radius of each drop was calculated as $r = \sqrt{\frac{A}{\pi}}$=13.9 $\pm$ 0.2 μm.

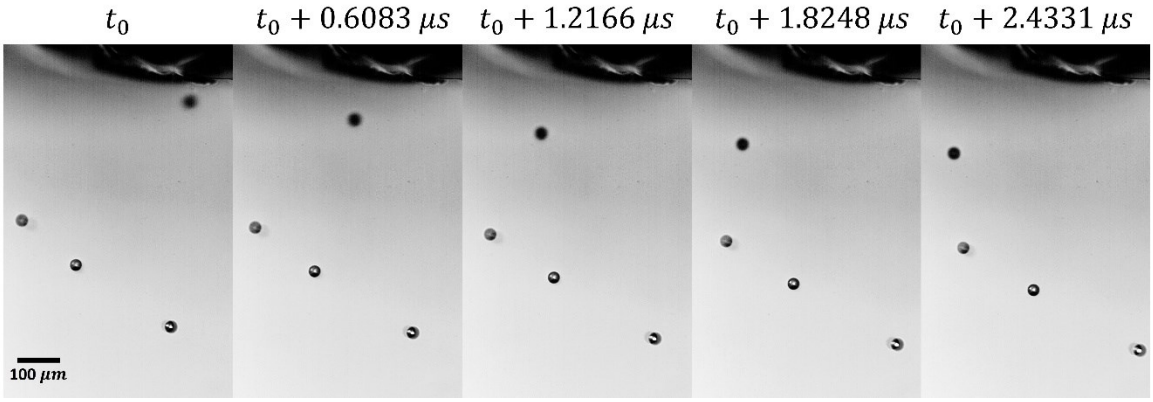

Fig. S1. Illustration of images used for evaluation of the drop volume.

In order to deposit each microdrop on the fiber, the position of the printing nozzle was adjusted by the 3D micromanipulator in the XZ-plane making small steps toward the fiber until we observed that the drop hit the top surface of the fiber. Then, the position of the nozzle was not changed anymore during experiments.

Before each experiment, we moved the fiber along its length to find a clean area for the drop placement, then we turned on the microdrop dispenser. Each experiment was repeated at least 5 times. Videos were recorded at 50 fps for those tubes with an advancing contact angle smaller than 40°. For advancing contact angles larger than 40° , the growth of the drop was recorded at 25 fps. The process of clamshell-barrel transition was recorded at 500 fps. When the transition from clamshell to barrel happened, we immediately stopped printing.

The critical drop volume required for the transition can be evaluated as follows $V = V_d \times t_{transit} \times f$, where V_{drop} is the volume of a single drop printed by the nozzle, $t_{transit}$ is the time counted from the first drop printed on the fiber to the moment when the transition has finished, and f is the printing frequency.

S2. Surface treatment and contact angle measurements

The capillary tubes were equally cut into two pieces. Both open ends of the tube were sealed for further contact angle characterization. We cleaned samples in methanol for 5 mins to remove the finish. Then the dried samples were placed in the plasma cleaner (PLASMA CLEANER/STERILIZER, Harrick Scientific Corp, PDC-32G, Input power 100 W, Highest settings: 720V DC, 25 mA DC, Applied to 18 W) to activate the surface. First, the chamber was vacuumized with an external vacuum pump. When the millitorr vacuum gauge showed that the pressure inside the chamber was under 200 mTorr, the PLASMA CLEANER/STERILIZER was

turned on and set it to High. The vacuum pump was still working. The plasma treatment took 15 minutes. Then, the plasma cleaner and the vacuum pump were turned off and the chamber was aired.

The samples were taken out from the chamber and immediately put into 50 ml centrifuge tubes (CELLTREAT Scientific Products) with different silanes present. All samples were left in the sealed centrifuge tubes for about 12 hours to graft silanes on the surface.

Besides the capillary tubes, the Basalt fibers (FibreCoat GmbH) of about 21 microns in diameter were used in these experiments. Since the wetting force acting on the fiber is too small to be detected by the force tensiometer, the receding/advancing contact angles between the fiber and the hexadecane were analyzed using the meniscus shape from the image sequences of the fiber being withdrawn/immersed vertically from/in the hexadecane bath. Figure 4 demonstrates the results of the best fitting of meniscus surface on the Basalt fiber using advancing contact angle $47 \pm 1°$. This angle remains the same after 3 repeats. Receding contact angle was measured to be $32 \pm 2°$ after 3 repeats.

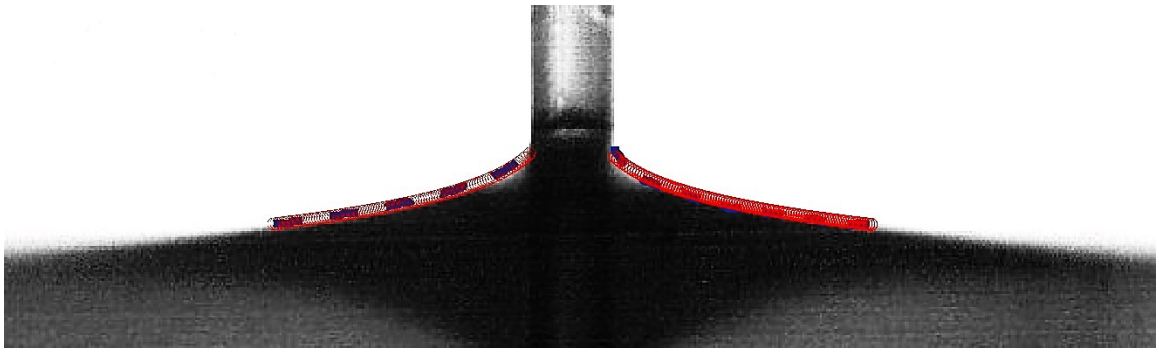

Fig.S2 The fiber that has been immersed vertically into hexadecane. The red curve shows the best-fit meniscus profile using the method of Refs. [42, 43]. The blue dashed curves show the extracted meniscus profile by the LabView program "IMAQ Extract Contour VI". These fitting provides 47° advancing contact angle with hexadecane on the left and 49° on the right sides.

Table S1. Contact angles measured on both sides of asymmetric barreled hexadecane drops

silane	Advancing CA[°]	Top CA[°]	Receding CA[°]	Bottom CA[°]
2-[Methoxy(Polyethyleneoxy)6-9propyl]trimethoxysilane	22±2	23±2	18±3	17±2
Methacryloxypropyltrimethoxysilane	29±2	31±1	19±3	19±2
UNTREATED TUBES	35±2	33±2	27±1	22±2
n-Octyldimethylchlorosilane	44±2	46±2	34±2	36±2
Basalt fiber	47±1	47±2	32±2	37±3

To measure the contact angles of asymmetric droplets, we developed an image processing protocol as follows. The formed droplets are mirror-symmetric with respect to the picture plane therefore, these contact angles can be related to the measured contact angles. Fitting the drop profile next to the contact line with a second-order polynomial function, as shown in Fig. S3, we inferred the contact angles.

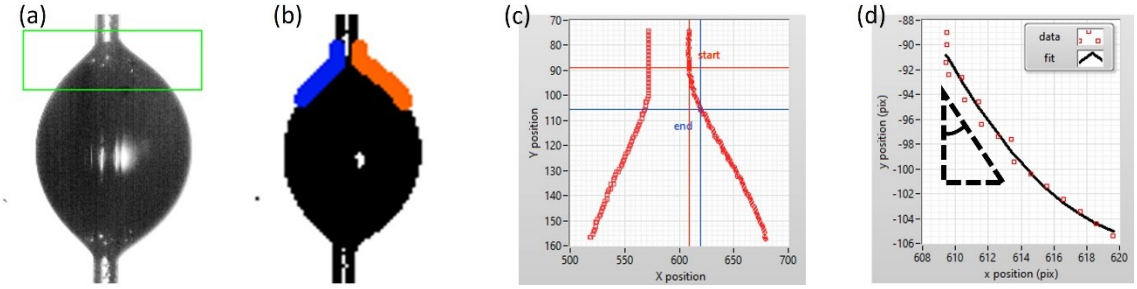

Fig. S3 (a)Selected region at the contact line. (b)Binarized image and extracted meniscus profiles. (c)The position of contact line has been specified and the 10 pixels-wide-band for profile fitting was determined. (d)The second order polynomial is applied to fit the profile and its derivative at the contact line gives the best-fit angle of 47°.

To deposit a liquid film that is thick enough for formation of a big liquid barrel, we used pure viscous glycerol (Glycerin 99.7%, Laboratory Reagent, VWR Chemicals BDH®). The inner surface of the feeding tube was chosen wettable, allowing us to trap the liquid inside it when we kept the tube horizontal. The receding contact angles between coated tubes and glycerol were

measured using K100 Force Tensiometer (KRÜSS) at a constant low speed of 0.3 mm/min to eliminate the effect of viscous force. The results are given in Table 1.

The receding contact angles between coated tubes and glycerol were measured using K100 Force Tensiometer (KRÜSS) at a constant low speed of 0.3 mm/min to eliminate the effect of viscous force. The results are given in Table S2.

Table S2. The contact angle between glycerol and capillary tubes.

tube O.D.[mm]	**Silane**	**Receding CA[°]**
0.25	2-[Methoxy(Polyethyleneoxy)6-9propyl]trimethoxysilane	25±2
0.25	UNTREATED TUBES	28±2
0.25	Methacryloxypropyltrimethoxysilane	38±1
0.25	(3-Glycidyloxypropyl)trimethoxysilane	40±3
0.17	n-Octyldimethylchlorosilane	60±2

S3. Printed droplets

Figure S4 shows how the drop shape changes as its volume increases. The zero-second picture indicates the shape of the very first drop just after its deposition on the fiber. After that, the drop starts to grow fed by the impacting microdroplets. While growing, it spreads over the fiber top side (0 S – 6 S in Fig. S4). Then, the clamshell propagates from the top to the fiber sides. When the drop volume reaches its critical value and the contact angle allows the clamshell to move toward the fiber bottom, it will suddenly transform to a barrel drop. Finally, an almost axisymmetric

barreled drop is formed on the fiber; at this moment the printing stops and the drop rests in this equilibrium configuration (57 s in Fig. S4).

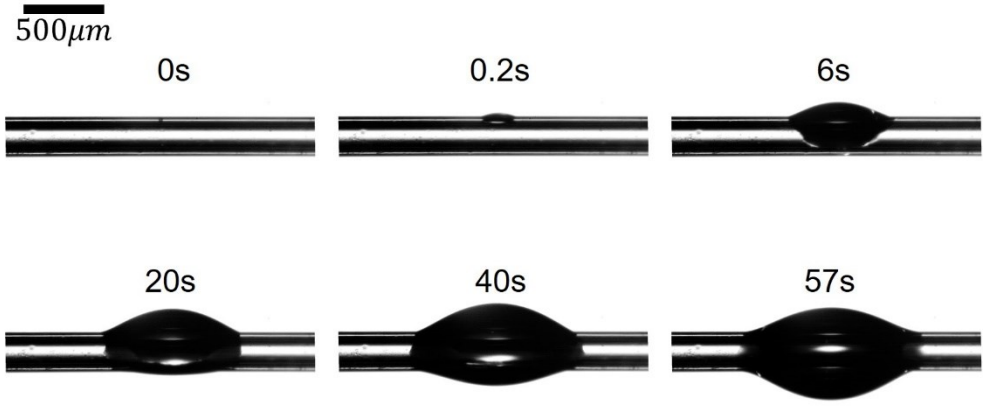

Fig. S4. An illustration of the clamshell-barrel transition using a hexadecane drop growing on a capillary tube of $2R_f$ =250 μm diameter. Hexadecane makes 37° advancing contact angle and 28° receding contact angle with the tube.

S3.1 Medium advancing contact angles, $\theta_{adv} = 35°$

An interesting transition mode could sometimes be observed during experiments with this capillary tube. This mode had never been observed in tubes with smaller contact angles. As shown in Fig. S5(b), from 50.00 s to 60.00 s, the clamshell rolled over the tube slowly and eventually sat on the bottom of the tube. One notices that the drop shapes at 50 s and 54 s in Fig S5 (b) are very close to that at 56.94 s in Fig. 3(a), which is the first frame of the sequence in Fig 3(a) of the main text. Instead of becoming a barrel drop immediately after rolling over the fiber, the clamshell on the bottom side kept growing for 5.08 s (60.00 s to 65.08 s in Fig. S5(b)), then suddenly transited to the barrel shape (65.08 s to 65.22 s in Fig. S5(b)). These observations suggest that the clamshell drop remains stable until it reaches a critical volume, even if one purposely wets the dry bottom of the clamshell drop.

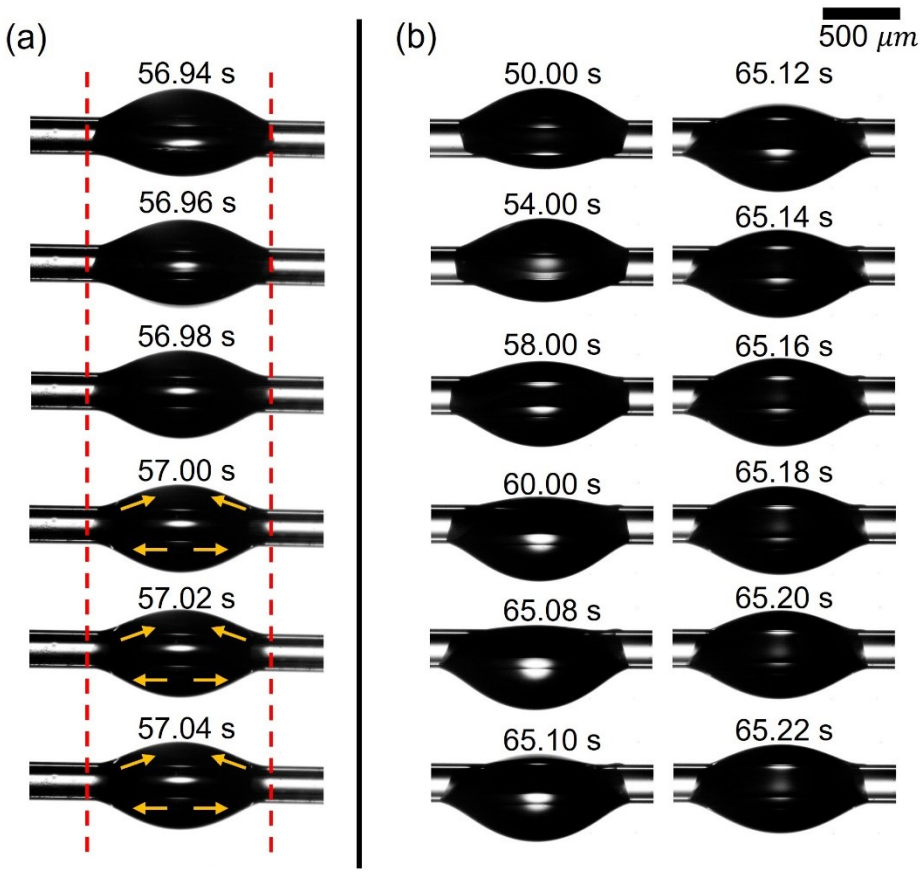

Fig. S5 (a) A hexadecane drop transits from the clamshell shape to the barrel shape on a capillary tube of $2R_f = 250\ \mu m$ diameter at 35° advancing contact angle. (b) The hexadecane clamshell drop was deposited from above on the tube top. Then the drop rolled from the top to the bottom of the tube and kept growing. The clamshell eventually became a barrel drop.

Figure S6 illustrates this transition on the Basalt fiber. The transition was completed in 4 ms. At the beginning of the transition, the contact lines were still pinned; however, the contact line slightly extended right before the transition finished.

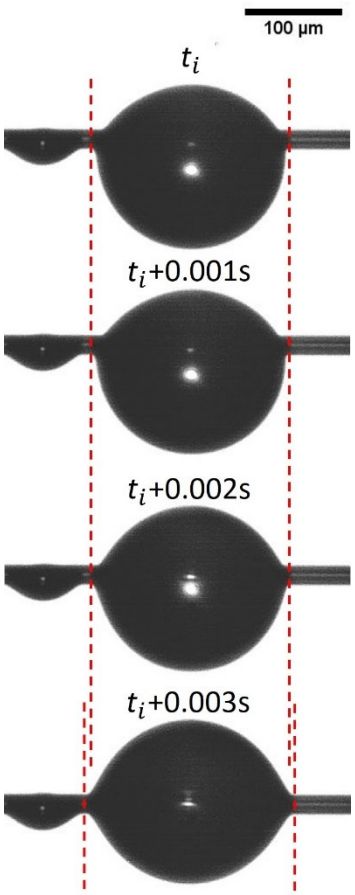

Fig. S6. A hexadecane drop transit from clamshell to barrel on Basalt fiber of $2R_f$ =42 μm diameter at 47° advancing contact angle. There is no connecting film between the smaller and larger droplets. Therefore, the contact line when it advances, moves over the dry surface of this fiber.

In Figure S7 (a), the relation between the critical ratio n and the measured advancing contact angles is shown by the blue crosses, with the error bars calculated as the half-value width of their standard deviations measured in experiments. In Figure S7(b), we plot the dimensionless volume, V/R_f^3 for the first barreled drop versus advancing contact angle.

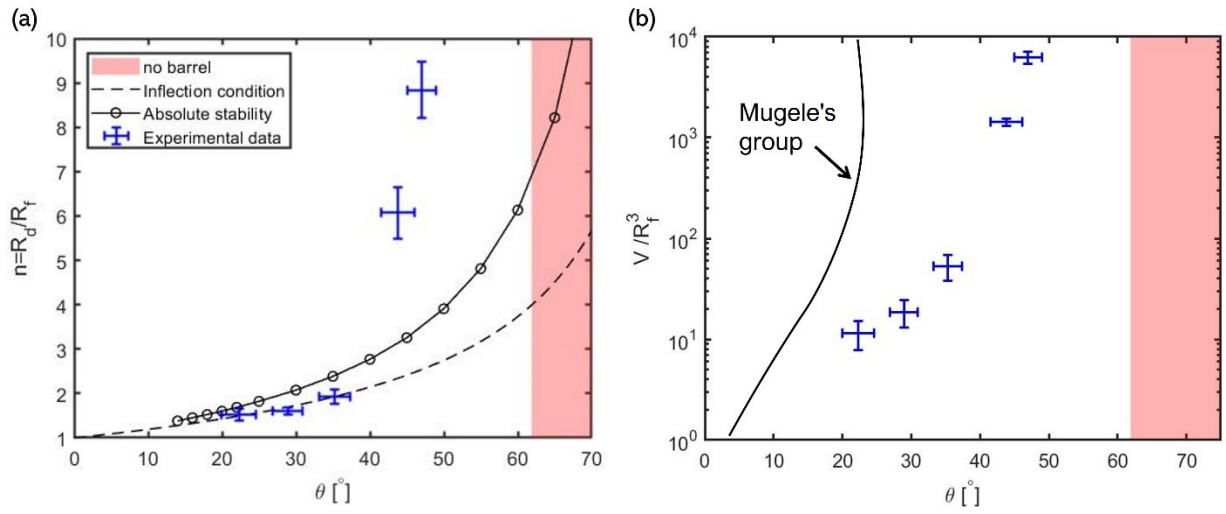

Fig. S7 (a) The diagram showing the transition boundary between the barrel and clamshell drop: (1)The dashed curve represents the inflection point condition[10], (2)the circles represent the absolute stability criterion[25], and (3)the blue crosses formed by the error bars show the experimentally observed dimensionless radius n of the critical barreled drop. The red shadow area indicates the no barreled drop region. (b) Dimensionless critical volume for the first barreled drop versus advancing contact angle. Comparison with the electrowetting experiments[9].

S4. Bond numbers

The Bond number was introduced as, $Bo = \frac{\rho g R_d^2}{\sigma}$, where ρ is the density of hexadecane, σ is the surface tension of hexadecane, R_d is the radius of critical barreled drop indicating the clamshell-barrel transition. To check with the Bond number introduced in Ref.[8], we added the column $Bo = \rho g R_f^2/\sigma$. Our experiments were conducted at the Bond numbers much smaller than those in Ref[8]. According to the theory, the smaller the Bond number, the smaller should be the drop asymmetry[8]. Thus, in experiments with extremely small Bond numbers, the drop deformation (for example, the difference in the bulge radius at the top and bottom sides of this drop) is expected to be of the order of $\sim Bo \cdot R_f$, i.e. it should not be detectable with the used microscope. Surprisingly, as shown in in Figs. 4(d) and (e), the more asymmetric drops correspond to the smaller Bond numbers at almost the same contact angles. Thus, the required trend for the gravity-

induced deformations is not there. Moreover, if the gravity causes this asymmetry, then the bottom side of the asymmetric drop should always be greater than the top side, which is clearly not true in our experiments.

Table S3 The Bond numbers formulated with R_d and R_f for critical barreled drops

Surface	**Advancing CA[°]**	**Bond Number** $\boldsymbol{Bo = \frac{\rho g R_d^2}{\sigma}}$	$\boldsymbol{Bo = \frac{\rho g R_f^2}{\sigma}}$
1	22 (2)	0.010	4.4×10^{-3}
2	29(2)	0.011	4.4×10^{-3}
3	37(2)	0.016	4.4×10^{-3}
4	44(2)	0.016	4.3×10^{-4}
5	47(2)	0.002	2.7×10^{-4}